Exploring light-by-light scattering with next-generation detectors

Antoni Szczurek
Institute of Nuclear Physics PAN, Kraków, Poland

in collaboration with P. Jucha, M. Klusek-Gawenda
based on:
arXiv:2308.01550

European Physical Society Conference on High Energy Physics (EPS-HEP 2023)
21st - 25th August 2023, Hamburg, Germany

Introduction

- $\gamma\gamma \to \gamma\gamma$ scattering is fully quantal effect.
- Several mechanisms can be present in principle.
- It was/is a dream for the laser community.
  Some works in this direction are going on.
- It was proposed by: D. d'Enterria, G. Silveira to do it in heavy ion UPC in 2013 (box diagrams only)
- M. Klusek-Gawenda, P. Lebiedowicz and A. Szczurek made an update in 2016. Different result numerically and a double-hadronic excitation (virtual vector mesons), called by us VDM Regge, was discussed.
- M. Klusek-Gawenda, W. Schafer and A. Szczurek, two-gluon exchange mechanism.
- ATLAS and CMS performed such experiments and got results consistent with our predictions.
- M. Klusek-Gawenda and A. Szczurek considered a background contribution: $\gamma\gamma \to \pi^0(\to 2\gamma)\pi^0(\to 2\gamma)$, also in $AA \to AA\pi^0\pi^0$.
- M. Klusek-Gawenda, R. McNulty, R. Schicker and A. Szczurek studied what ALICE and LHCb could do.
- There are at least two experimental projects that could provide new insights into photon-photon scattering: FoCal and ALICE 3.

Sketch of the formalism, EPA

The nuclear cross section is calculated using equivalent photon approximation (EPA) in the b-space. In this approach, the di-photon cross section can be written as:

$$\begin{aligned}\frac{d\sigma(PbPb \to PbPb\gamma\gamma)}{dy_{\gamma_1}\, dy_{\gamma_2}\, dp_{t,\gamma}} &= \int \frac{d\sigma_{\gamma\gamma\to\gamma\gamma}(W_{\gamma\gamma})}{dz} N(\omega_1, b_1) N(\omega_2, b_2) S^2_{abs}(b) \\ &\times d^2 b d\bar{b}_x d\bar{b}_y \frac{W_{\gamma\gamma}}{2} \frac{dW_{\gamma\gamma} dY_{\gamma\gamma}}{dy_{\gamma_1}\, dy_{\gamma_2}\, dp_{t,\gamma}} dz \,, \end{aligned} \tag{1}$$

where $\bar{b}_x = (b_{1x} + b_{2x})/2$ and $\bar{b}_y = (b_{1y} + b_{2y})/2$. The relation between $\vec{b}_1$, $\vec{b}_2$ and impact parameter: $b = |\vec{b}| = \sqrt{|\vec{b}_1|^2 + |\vec{b}_2|^2 - 2|\vec{b}_1||\vec{b}_2|\cos\phi}$. Absorption factor $S^2_{abs}(b)$ is calculated as:

$$S^2_{abs}(b) = \Theta(b - b_{max}) \tag{2}$$

or

$$S^2_{abs}(b) = exp\left(-\sigma_{NN}\, T_{AA}(b)\right) , \tag{3}$$

where σ_{NN} is the nucleon-nucleon interaction cross section.

Sketch of the formalism, EPA

$T_{AA}(b)$ above is related to the so-called nuclear thickness, $T_A(b)$,

$$T_{AA}\left(|\vec{b}|\right) = \int d^2\rho\, T_A\left(\vec{\rho} - \vec{b}\right)\, T_A\left(\vec{\rho}\right), \tag{4}$$

and the nuclear thickness is obtained by integrating the nuclear density

$$T_A\left(\vec{\rho}\right) = \int \rho_A\left(\vec{r}\right) dz, \qquad \vec{r} = \left(\vec{\rho}, z\right) \ , \tag{5}$$

where ρ_A is the nuclear charge distribution.

The nuclear photon fluxes $N(\omega_1, b_1)$ and $N(\omega_2, b_2)$ are calculated with realistic charge distribution.

Mechanisms of photon-photon scattering

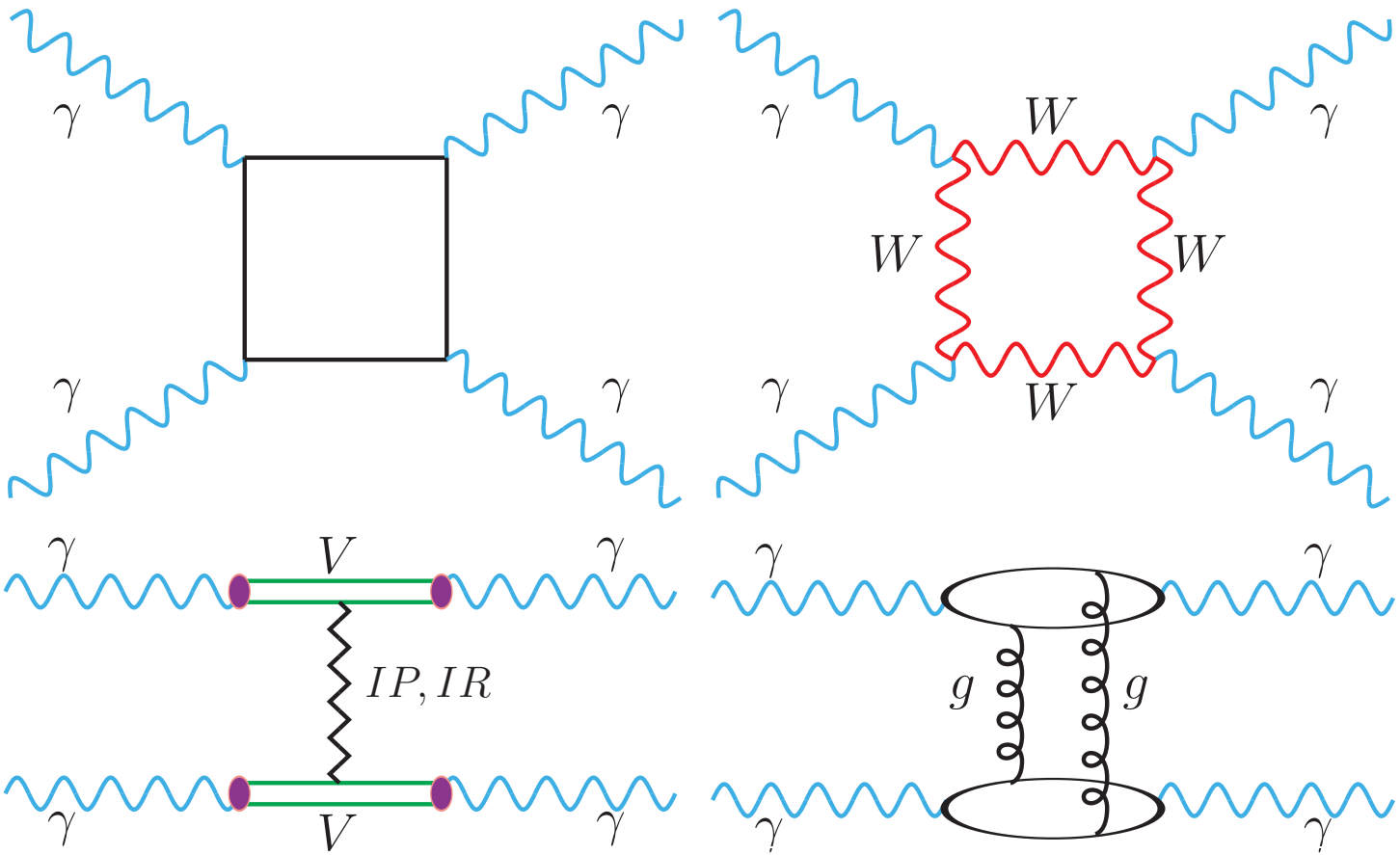

Elementary cross section

The elementary cross section here is calculated for unpolarised photons. To do this, all 16 photon helicity combinations of the cross section must be added up. In fact, due to symmetries, it is sufficient to count only five combinations and then add them up with the corresponding weights:

$$\Sigma_{helicities}|\mathcal{A}_{\gamma\gamma\to\gamma\gamma}|^2 = 2|\mathcal{A}^{fermions}_{++++}|^2 + 2|\mathcal{A}^{fermions}_{+--+}|^2$$

$$+2 \mid \mathrm{A}^{fermions}_{+-+-}|^2 + 2|\mathcal{A}^{fermions}_{++--}|^2 + 8|\mathcal{A}^{fermions}_{+-++}|^2 \ . \quad (6)$$

Elementary cross section calculations for the box contribution were carried out using FormCalc and LoopTools libraries based on Mathematica software.

Elementary cross section, VDM

This component was calculated for the first time by Klusek-Gawenda, Lebiedowicz, Szczurek 2016 assuming vector dominance model. In this approach, the amplitude is:

$$\begin{aligned}\mathcal{M} &= \Sigma_{i,j} C_i^2 C_j^2 \left(C_{\mathbb{P}} \left(\frac{s}{s_0}\right)^{\alpha_{\mathbb{P}}(t)-1} F(t) + C_{\mathbb{R}} \left(\frac{s}{s_0}\right)^{\alpha_{\mathbb{R}}(t)-1} F(t) \right) , \\ &+ \Sigma_{i,j} C_i^2 C_j^2 \left(C_{\mathbb{P}} \left(\frac{s}{s_0}\right)^{\alpha_{\mathbb{P}}(u)-1} F(u) + C_{\mathbb{R}} \left(\frac{s}{s_0}\right)^{\alpha_{\mathbb{R}}(u)-1} F(u) \right) . \end{aligned} \quad (7)$$

In the simplest version of the model $i, j = \rho^0, \omega, \phi$ (only light vector mesons are included). The couplings C_i, C_j describe the $\gamma \to V_{i/j}$ transitions that are calculated based on vector meson dilepton width. $C_{\mathbb{P}}$ and $C_{\mathbb{R}}$ are extracted from the Regge factorization hypothesis (Szczurek, Nikolaev, Speth).

It was shown that the component is concentrated mainly at small photon transverse momenta which at not too small subsystem energies corresponds to $z \approx \pm 1$. The Regge trajectories are usually written in a linear form:

$$\begin{aligned}\alpha_{\mathbb{P}}(t/u) &= \alpha_{\mathbb{P}}(0) + \alpha'_{\mathbb{P}} t/u , \\ \alpha_{\mathbb{R}}(t/u) &= \alpha_{\mathbb{R}}(0) + \alpha'_{\mathbb{R}} t/u . \end{aligned} \quad (8)$$

These linear forms are valid at not too large $|t|$ or $|u|$. At large $|t|$ or $|u|$ the energy dependent factors are artificially small. Therefore here where we explore it more, we propose to smoothly switch off the t/u dependent terms in (8) at $t \sim$ -0.5 GeV^2 and $u \sim$ -0.5 GeV^2.

Elementary cross section, VDM

We also wish to analyze whether the more heavy vector mesons such as J/ψ can give a sizeable contribution.
For example, for the double J/ψ fluctuations (both photons fluctuate into virtual J/ψ mesons) we take the following Ansatz for the helicity conserving amplitude:

$$\mathcal{M}^{J/\psi J/\psi}_{VDM} = g^2_{J/\psi} C^{J/\psi}_{\mathbb{P}} \left(\frac{s}{s_0}\right)^{\alpha^{J/\psi J/\psi}_{\mathbb{P}}(t)-1} F^H_{J/\psi J/\psi \mathbb{P}}(t) F^H_{J/\psi J/\psi \mathbb{P}}(t) \quad (9)$$

$$+ \; g^2_{J/\psi} C^{J/\psi}_{\mathbb{P}} \left(\frac{s}{s_0}\right)^{\alpha^{J/\psi J/\psi}_{\mathbb{P}}(u)-1} F^H_{J/\psi J/\psi \mathbb{P}}(u) F^H_{J/\psi J/\psi \mathbb{P}}(u) \; . \quad (10)$$

In this case (double J/ψ fluctuations) only pomeron can be exchanged (no subleading regeons are possible due to the $c\bar{c}$ structure of J/ψ mesons). In this case, for simplicity, we take the simplified trajectories as

$$\alpha^{J/\psi J/\psi}_{\mathbb{P}}(t) = \alpha^{J/\psi J/\psi}_{\mathbb{P}}(u) = \alpha^{J/\psi J/\psi}_{\mathbb{P}}(0) \; . \quad (11)$$

Here the t/u dependencies are totally ignored. In numerical calculations we take $\alpha^{J/\psi J/\psi}_{\mathbb{P}}(0) = 1.3$ - 1.4 (typical hard pomeron).

Elementary cross section, VDM

Since the J/ψ mesons are far off-mass-shell and more compact than light vector mesons also the form factors must be modified:

$$F^H_{J/\psi J/\psi \mathbb{P}}(t) = \exp\left(\frac{t - m^2_{J/\psi}}{\Lambda^2_{J/\psi}}\right) , \tag{12}$$

$$F^H_{J/\psi J/\Psi \mathbb{P}}(u) = \exp\left(\frac{u - m^2_{J/\psi}}{\Lambda^2_{J/\psi}}\right) . \tag{13}$$

Please note that the form factors are normalized to 1 on the meson (J/ψ) mass shell.
One could also use monopole-like form factors. These form factors drastically reduce the $J/\psi J/\psi$ component of the amplitude in comparison to light vector meson components.
However, due to compactness of J/ψ we expect $\Lambda_{J/\psi}$ to be large. In the calculations presented here, we take $\Lambda_{J/\psi} = 2$ GeV for illustration.
In a similar fashion, one could include one J/ψ fluctuation and one light vector meson fluctuation. However, there the choice of trajectories is unclear.

Elementary cross section, VDM

Finally, let us discuss the helicity structure of the double photon hadronic fluctuation amplitude. We write:

$$\mathcal{M}^{(t)}_{\lambda_1\lambda_2\to\lambda_3\lambda_4} = A(t)\,\delta_{\lambda_1\lambda_3}\delta_{\lambda_2\lambda_4}\ , \tag{14}$$

$$\mathcal{M}^{(u)}_{\lambda_1\lambda_2\to\lambda_3\lambda_4} = A(u)\,\delta_{\lambda_1\lambda_4}\delta_{\lambda_2\lambda_3}\ . \tag{15}$$

$A(t)$ and $A(u)$ are given explicitly in (7). Then the total double VDM amplitude, including t and u processes, reads:

$$\mathcal{M}^{VDM}_{\lambda_1\lambda_2\to\lambda_3\lambda_4} = \frac{1}{\sqrt{2}}\left(\mathcal{M}^{VDM,(t)}_{\lambda_1\lambda_2\to\lambda_3\lambda_4} + \mathcal{M}^{VDM,(u)}_{\lambda_1\lambda_2\to\lambda_3\lambda_4}\right)\ . \tag{16}$$

Having the double VDM helicity amplitudes, we can add different mechanisms coherently:

$$\mathcal{M}_{\lambda_1\lambda_2\to\lambda_3\lambda_4} = \mathcal{M}^{boxes}_{\lambda_1\lambda_2\to\lambda_3\lambda_4} + \mathcal{M}^{VDM}_{\lambda_1\lambda_2\to\lambda_3\lambda_4} + \mathcal{M}^{\pi^0}_{\lambda_1\lambda_2\to\lambda_3\lambda_4} + \dots\ . \tag{17}$$

In the following, we shall discuss the coherent sum of the larger two components (boxes and VDM) and quantify their interference effects.

Background contribution

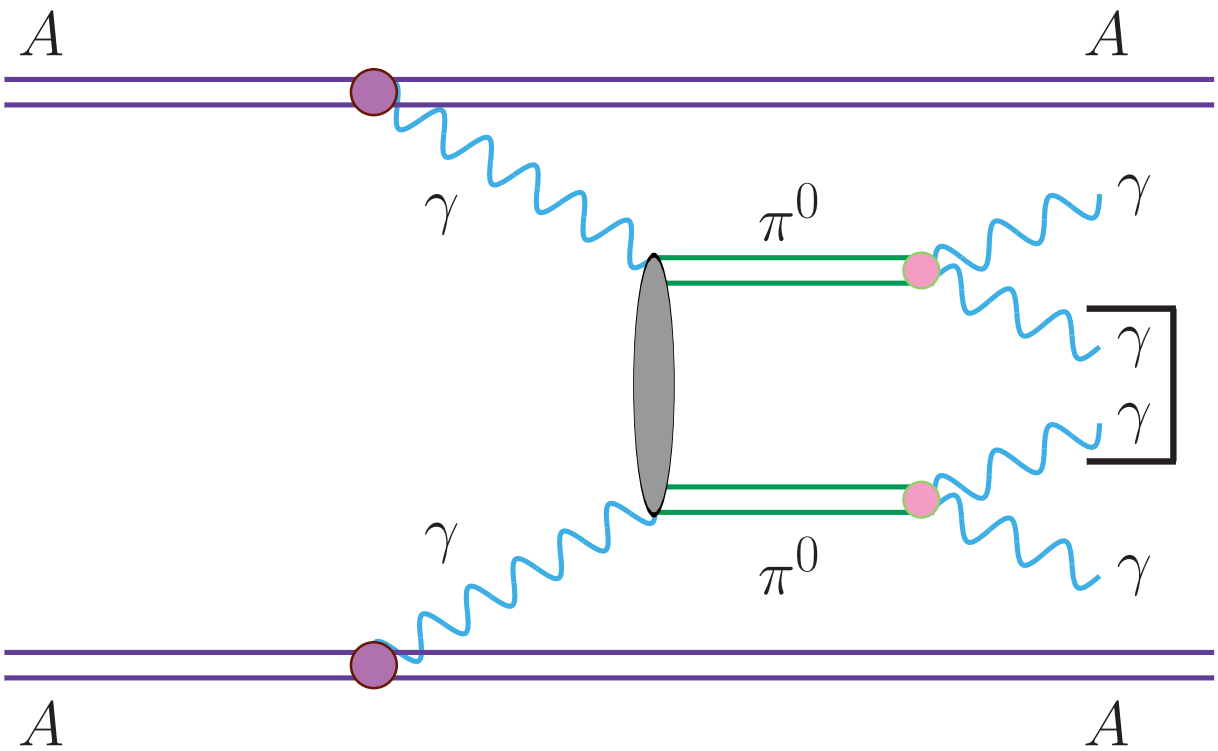

Figure: The dominant background contribution.

Background contribution

The $\gamma\gamma \to \pi^0(\to 2\gamma)\pi^0(\to 2\gamma)$ reaction constitutes a difficult background for the $\gamma\gamma \to \gamma\gamma$ measurements at intermediate $M_{\gamma\gamma}$. How to calculate the cross section for $\gamma\gamma \to \pi^0\pi^0$ reaction was discussed by Klusek-Gawenda, Szczurek 2013.

The calculation of the background proceeds in three steps.

- First the cross section for $\gamma\gamma \to \pi^0\pi^0$ is calculated.
- Next the cross section for $AA \to AA\pi^0\pi^0$ is computed in the equivalent photon approximation in an analogous way as described in the previous subsection.
- Finally the simulation of both π^0 decays is performed and combined distributions of one photon from the first π^0 and one photon from the second π^0 are constructed.

Results, elementary cross section

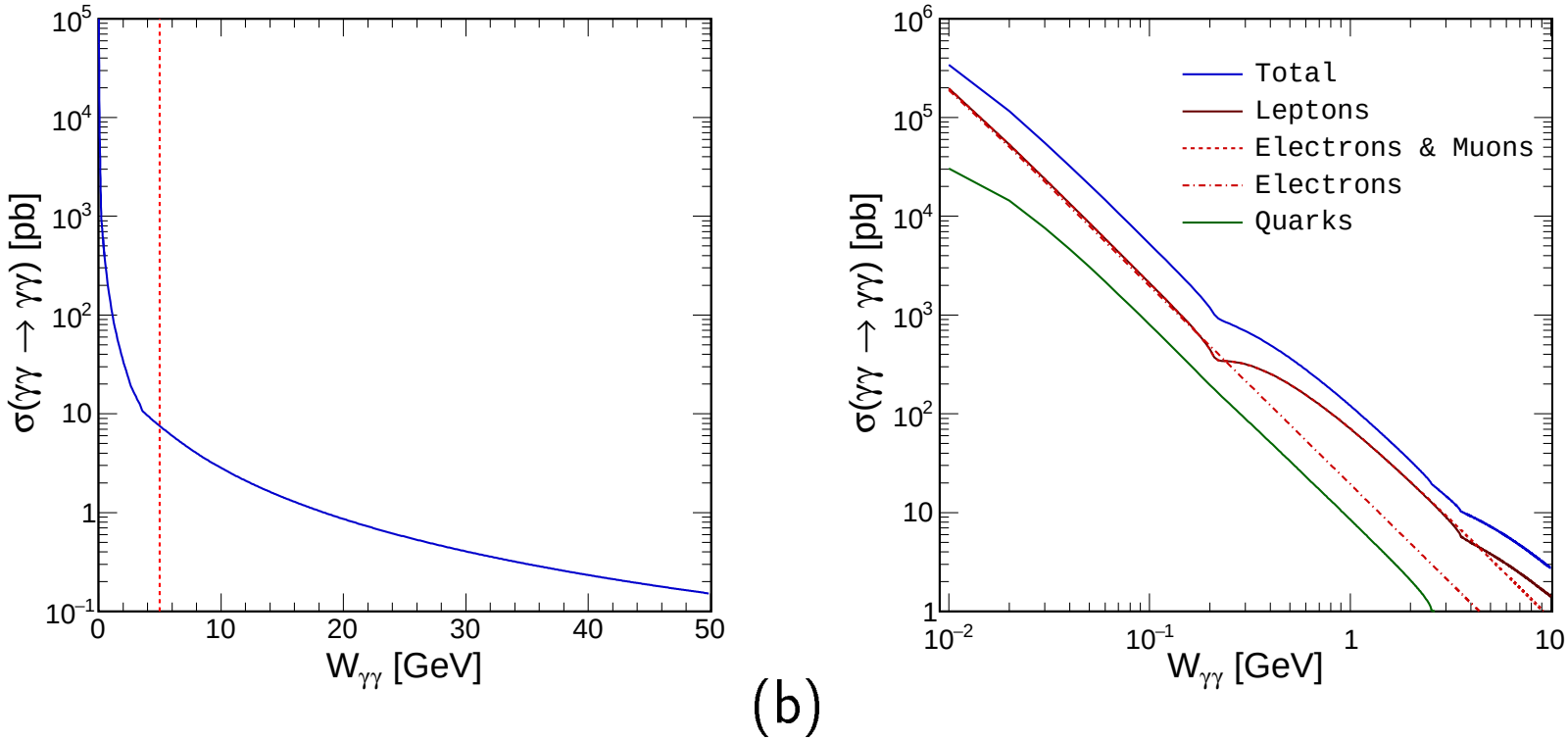

Figure: Elementary cross section (in pb) as a function of energy. Results for fermionic boxes are shown over a wide range of energies (a) MeV range (b). The total cross section (blue solid line) is split into quarks (green solid line), electrons (red dashed line), electrons and muons (red dotted line), and leptons (red solid line) contributions.

Results, elementary cross section

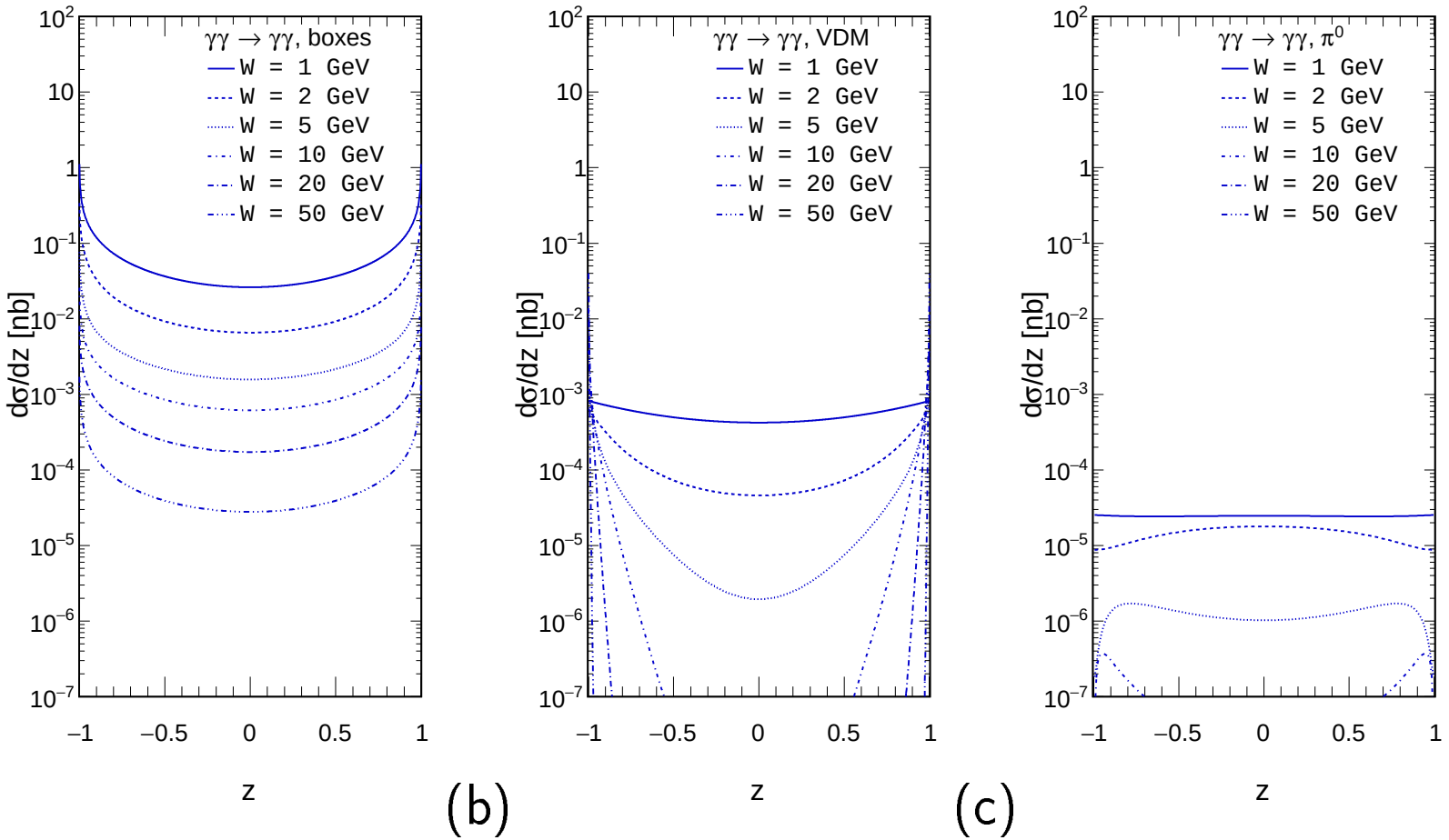

Figure: $cos(\theta)$ distributions for (a) boxes, (b) double hadronic fluctuations and (c) π^0 exchange for different energies $W = 1, 2, 5, 10, 20, 50$ GeV.

Results, elementary cross section

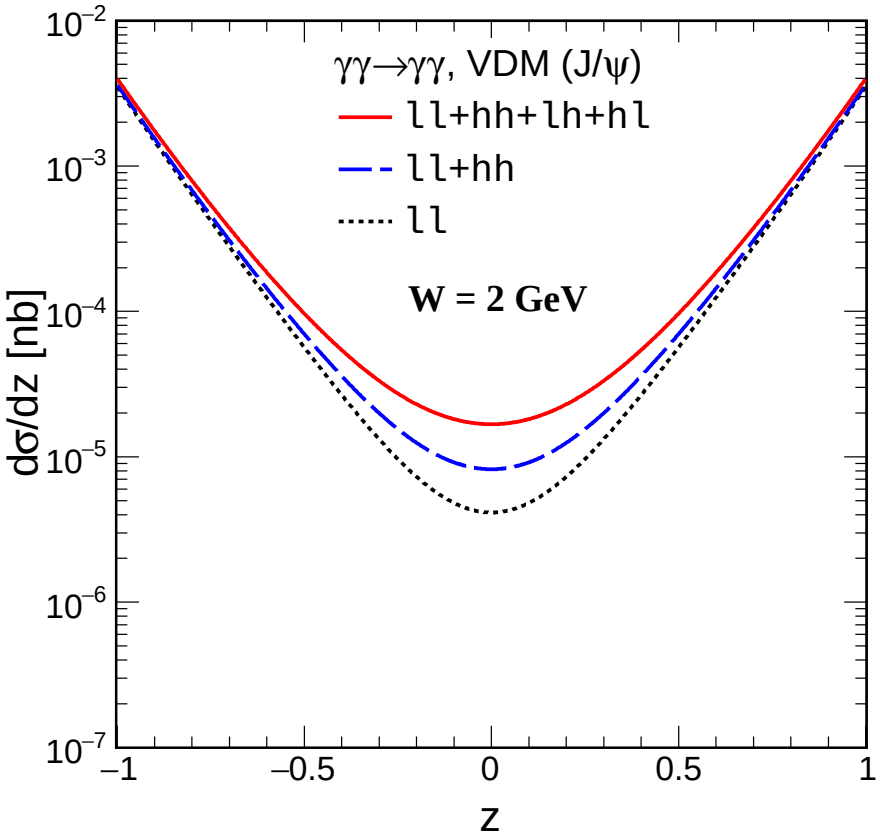

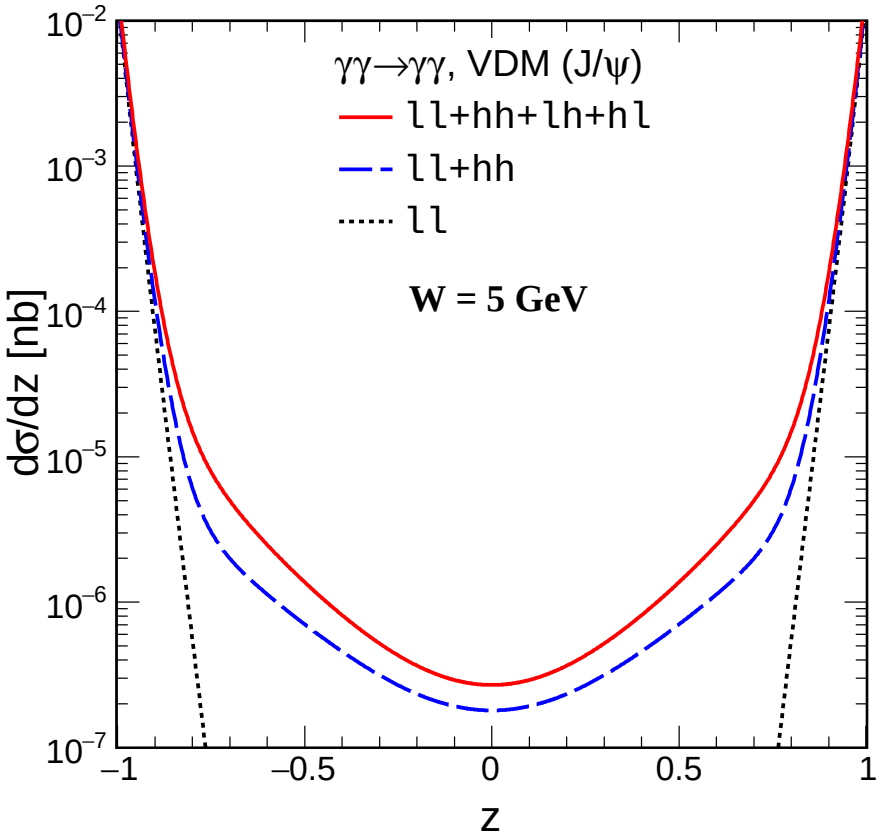

Figure: Including different photon fluctuations: $VV, J/\psi J/\psi, VJ/\psi, J/\psi V$. The effect disappers at $z \pm 1$. Here $C_{J/\psi J/\psi} = C_{VV}/4$ and $C_{J/\psi V} = C_{V,J/\psi}/2$.

Results, elementary cross section

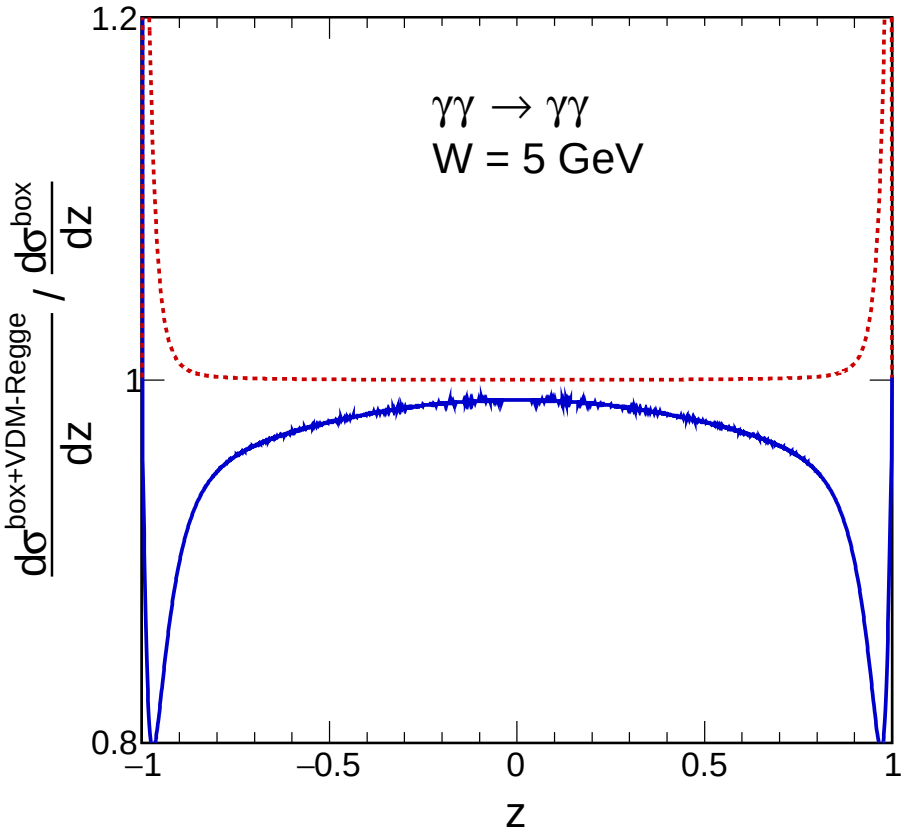

Figure: The ratio of the coherent (blue) and incoherent (red) sum of the box and VDM-Regge contributions divided by the cross section for the box contribution alone for $W = 5$ GeV.

Results - nuclear cross section

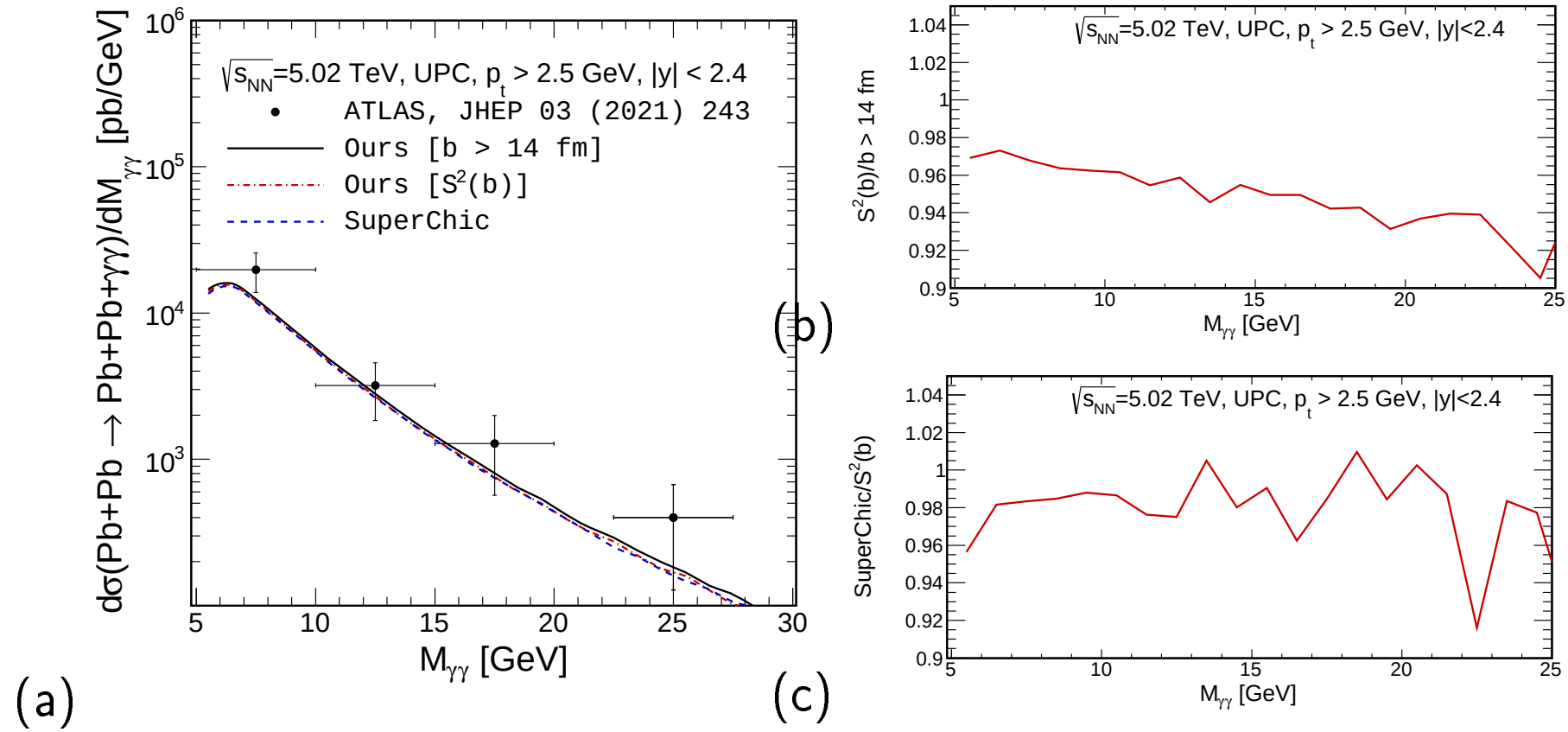

Figure: Differential cross section as a function of two-photon invariant mass at $\sqrt{s_{NN}} = 5.02$ TeV.
(a) The ATLAS experimental data are collected with theoretical results including a sharp cut on impact parameter ($b > 14$ fm - solid black line) and

Results - nuclear cross section

Experiment	$p_{t,min}$ [GeV]	UPC condition	σ_{tot} [nb]
ATLAS	2.5	b $>$ 14 fm	81.062 $\pm$ 0.05
		S^2(b) Eq. (3)	78.092 $\pm$ 0.05
		SuperChick	76.421 $\pm$ 0.074
CMS	2	b $>$ 14 fm	105.986 $\pm$ 0.067
		S^2(b)	102.104 $\pm$ 0.057
		SuperChick	100.101 $\pm$ 0.144

Table: Total cross section for PbPb$\to$PbPb$\gamma\gamma$ in nb obtained in different approaches for experimental ATLAS/CMS kinematics: collision energy $\sqrt{s_{NN}} = 5.02$ TeV, di-photon invariant mass $M_{\gamma\gamma} > 5$ GeV, photon rapidity $|y| < 2.4$. ATLAS and CMS detected photons in different range of transverse momenta.

Results - nuclear cross section

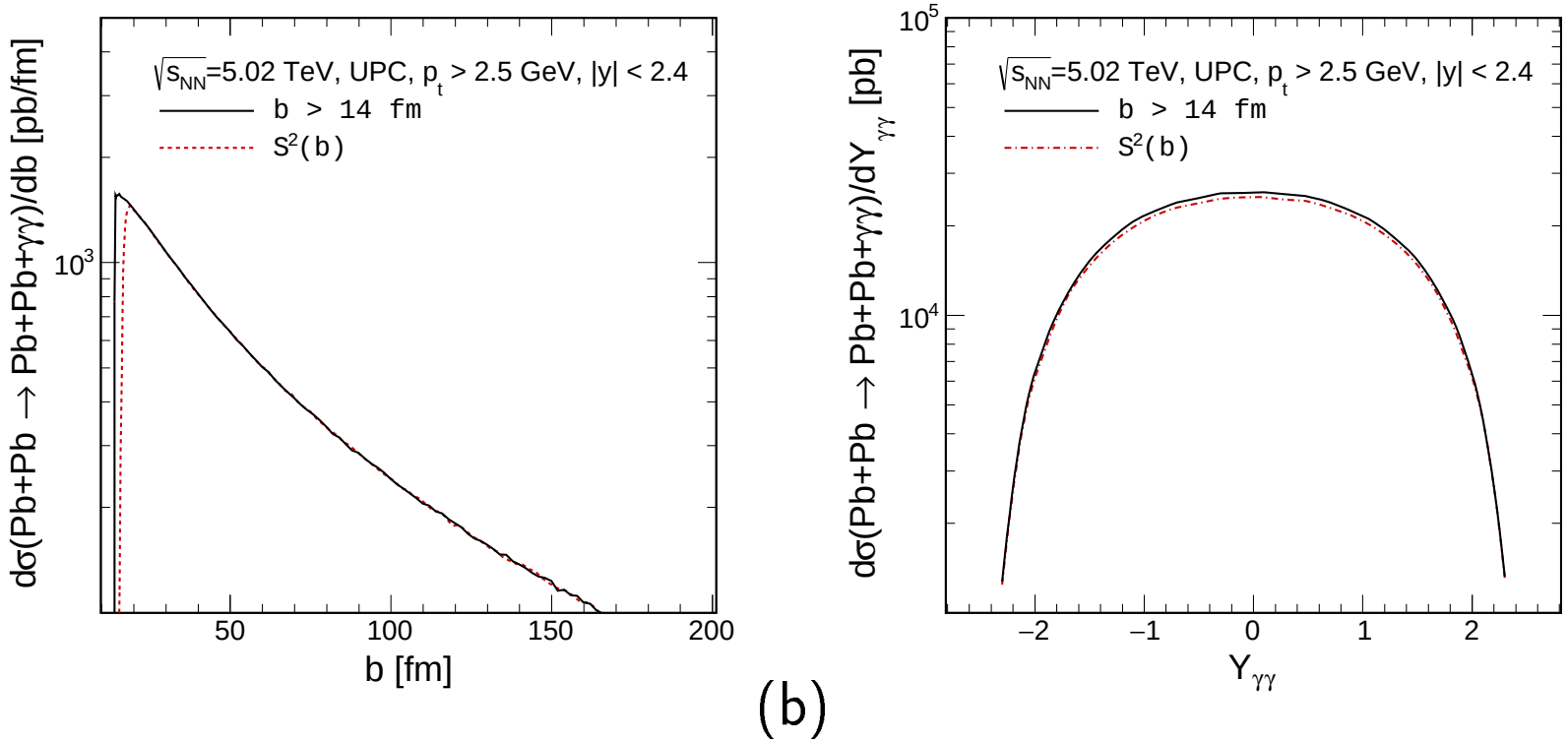

Figure: (a) Impact parameter and (b) rapidity distribution for UPC of lead-lead at collision energy $\sqrt{s_{NN}} = 5.02$ TeV. The solid line corresponds to a sharp cut on the impact parameter and the red dash-dotted line is for the absorption factor given by Eq. (3).

Broad range of rapidity, full phase space

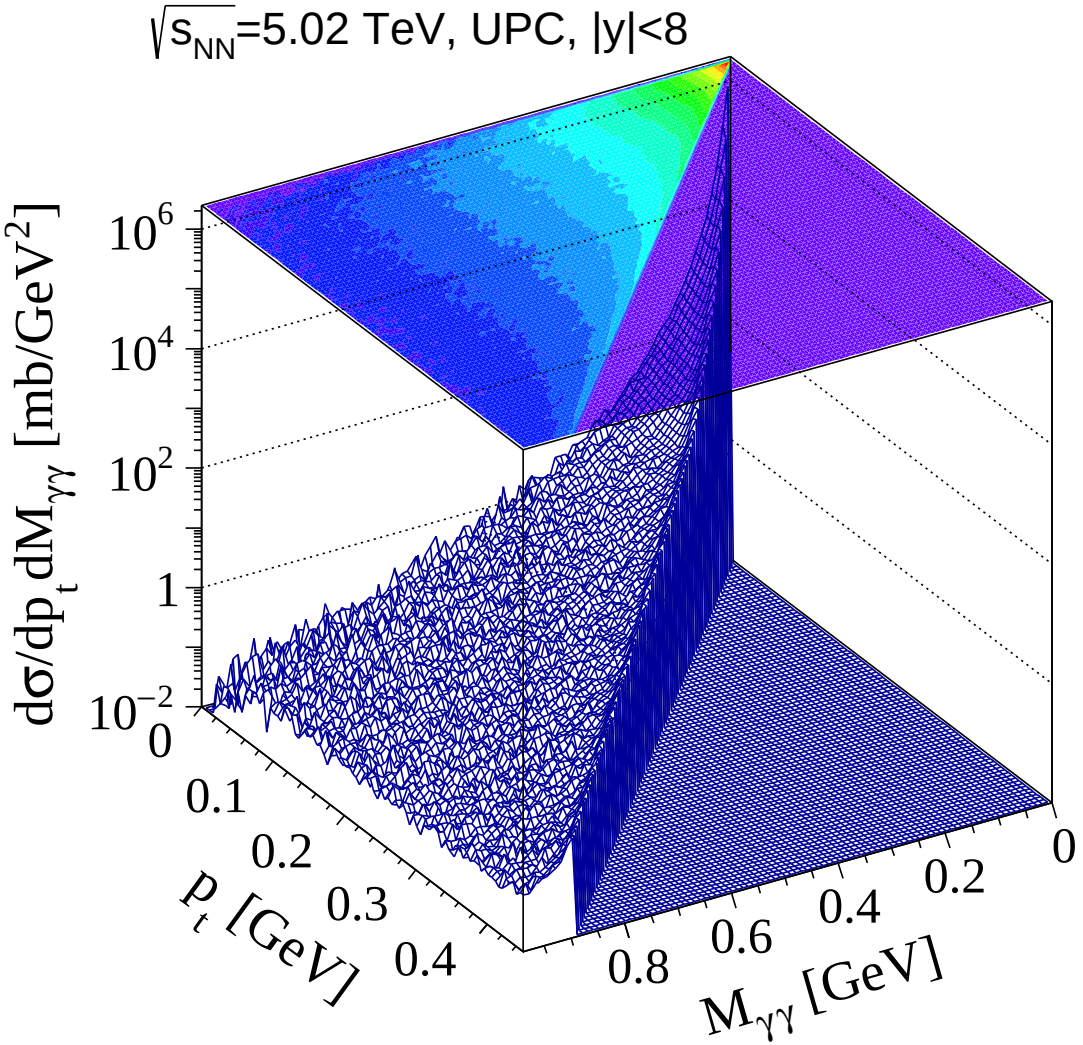

Broad range of rapidity, full phase space

	σ_{tot} [mb]
Total	91.675 $\pm$ 0.023
electrons+muons	41.597 $\pm$ 0.010
electrons	39.163 $\pm$ 0.010
quarks	12.483 $\pm$ 0.003

Table: Total cross section in mb for PbPb$\to$PbPb$\gamma\gamma$ for different fermionic contributions artificially separated. Here collision energy $\sqrt{s_{NN}} = 5.02$ TeV, di-photon invariant mass $M_{\gamma\gamma} \in (0.01 - 1)$ GeV, photon transverse momentum $p_t > 5$ MeV and photon rapidity $|y| < 8$.

Broad range of rapidity, full phase space

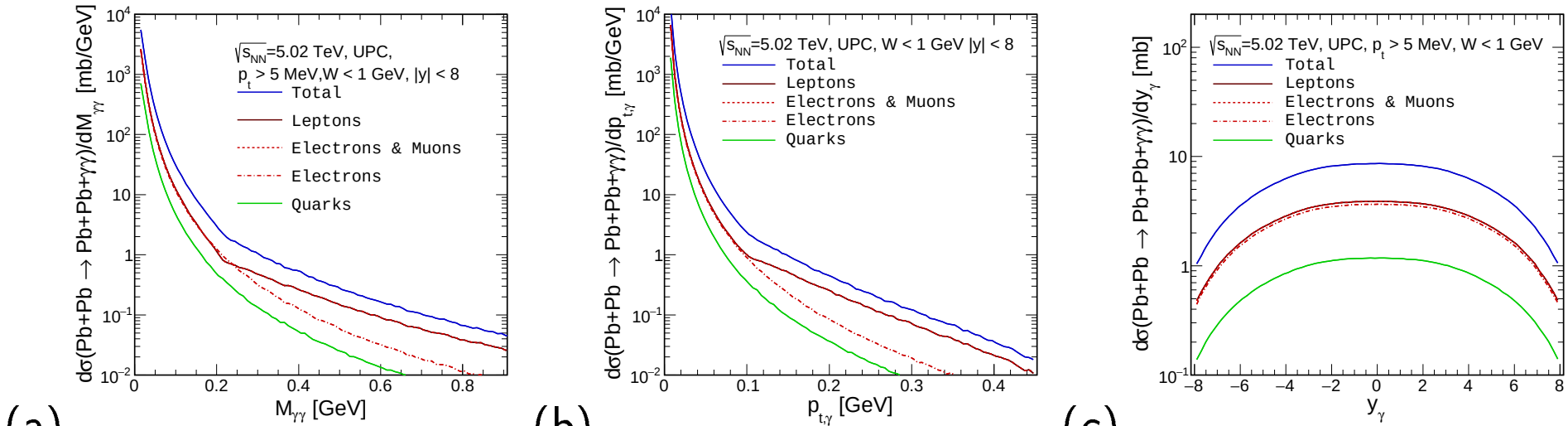

Figure: (a) Di-photon invariant mass, (b) photon transverse momentum and (c) rapidity distribution in mb for different fermionic contributions in ultraperipheral lead-lead collisions at energy $\sqrt{s_{NN}} = 5.02$ TeV. The blue solid line corresponds to a sum of all contributions, the red solid line is a sum for leptons, the dashed red line relates to electrons, and the green solid line represents quarks contribution.

Broad range of rapidity, full phase space

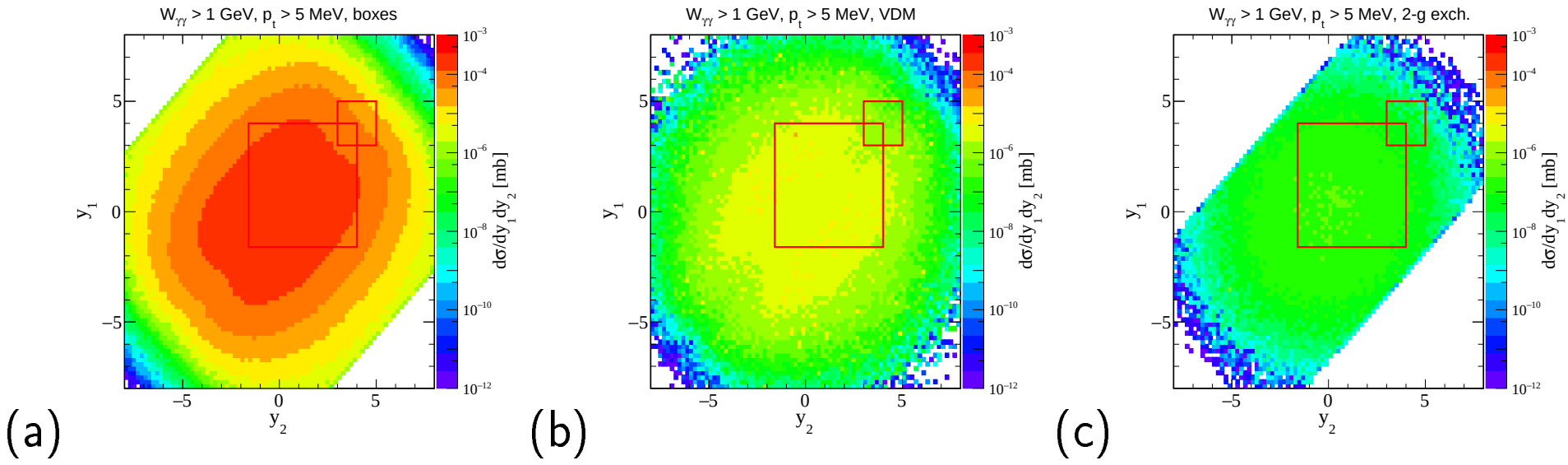

Figure: Distribution in (y_1, y_2) in mb for photon transverse momentum $p_t > 5$ MeV, di-photon invariant mass $M_{\gamma\gamma} > 1$ GeV.
(a) Boxes, (b) VDM-Regge and (c) two-gluon exchange.

Broad range of rapidity, full phase space

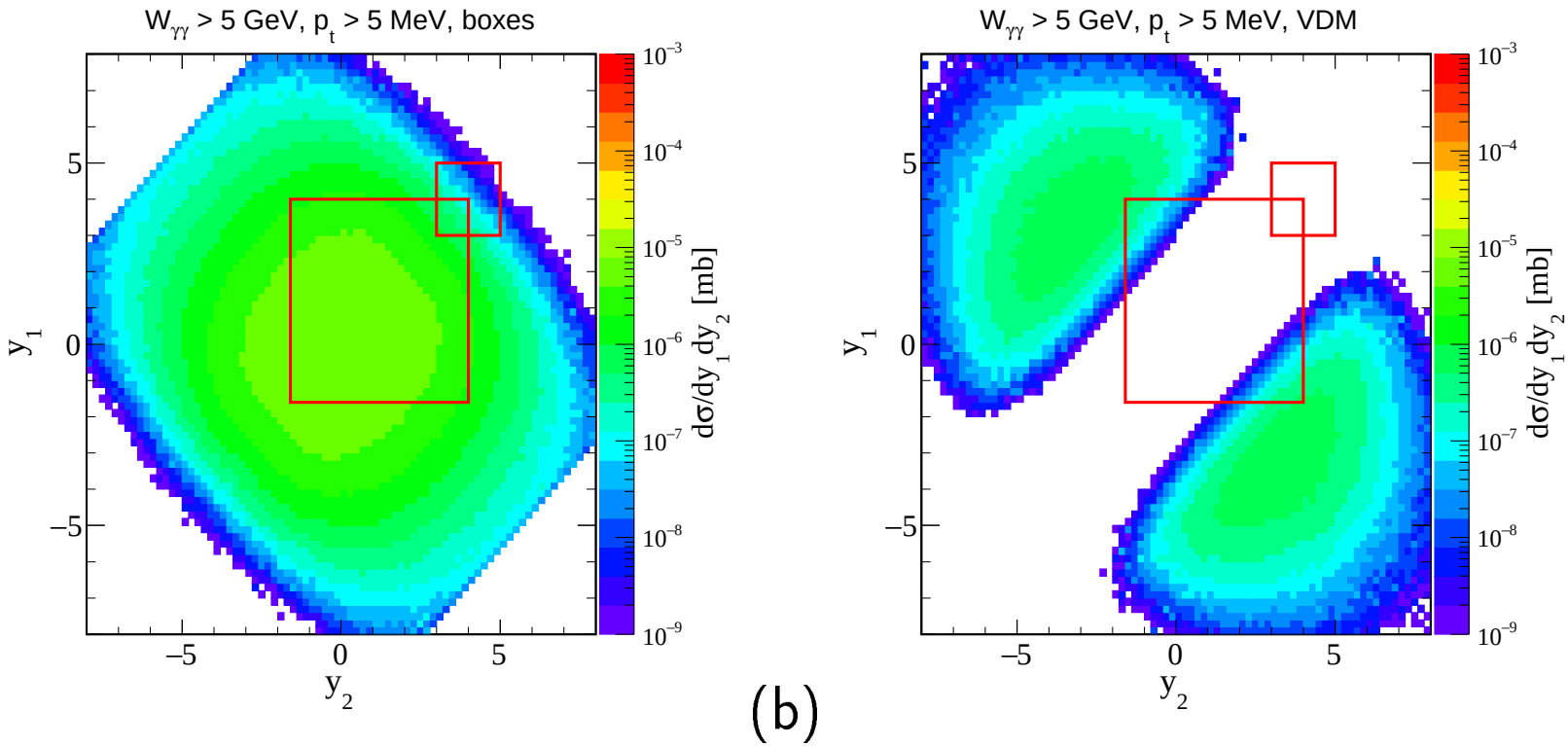

Figure: Distribution in (y_1, y_2) in mb for transverse momentum $p_t > 5$ MeV, di-photon invariant mass $M_{\gamma\gamma} > 5$ GeV.
(a) Boxes, (b) VDM-Regge mechanism.

Broad range of rapidity, full phase space

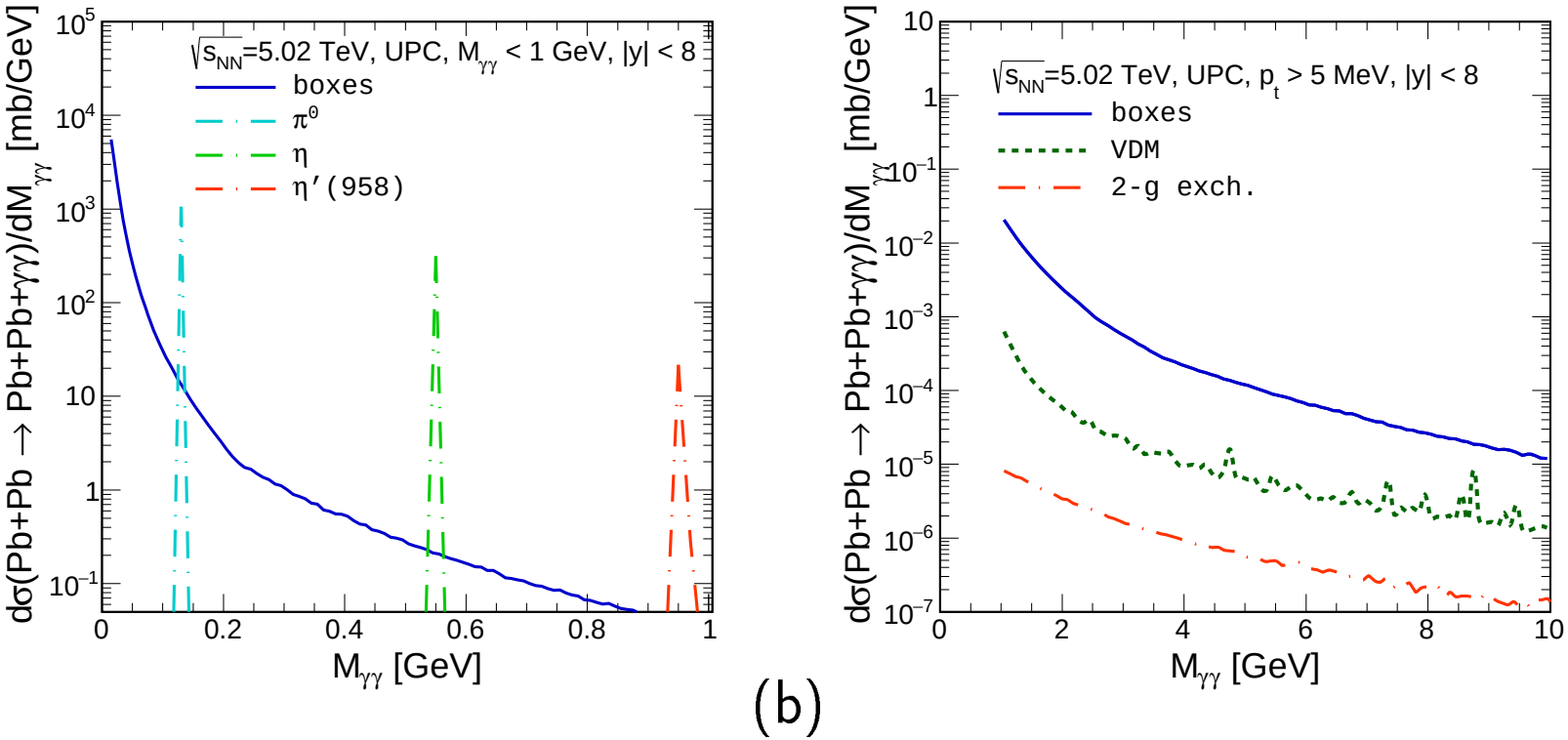

Figure: Di-photon invariant mass distribution for photon transverse momentum $p_t > 5$ MeV and photon rapidities $y_{1/2} \in (-8, 8)$.
(a) Boxes vs resonances, $M_{\gamma\gamma} < 1$ GeV (b) Boxes vs VDM-Regge and vs two-gluon exchange contribution, $M_{\gamma\gamma} > 1$ GeV.

Broad range of rapidity, full phase space

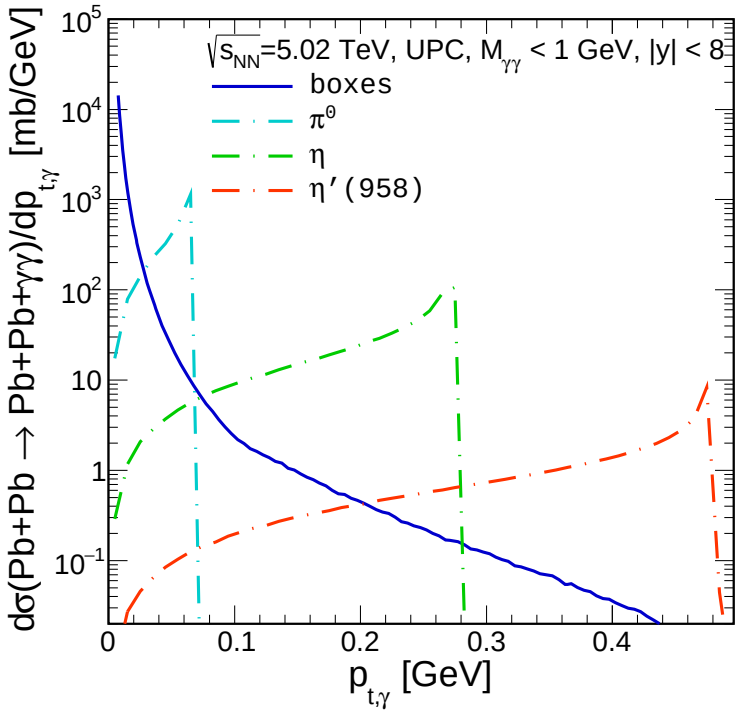

(a)

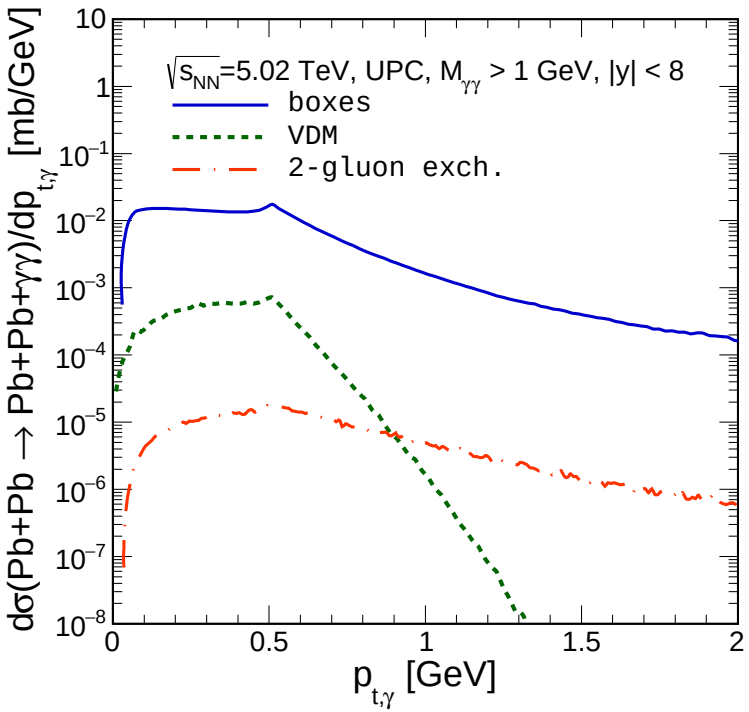

(b)

Figure: Transverse momentum distribution for photon transverse momentum $p_t > 5$ MeV, di-photon invariant mass $M_{\gamma\gamma} < 1$ GeV and photon rapidities $y_{1/2} \in (-8, 8)$.
(a) Boxes vs resonances; (b) boxes vs VDM-Regge vs two-gluon exchange.

Broad range of rapidity, full phase space

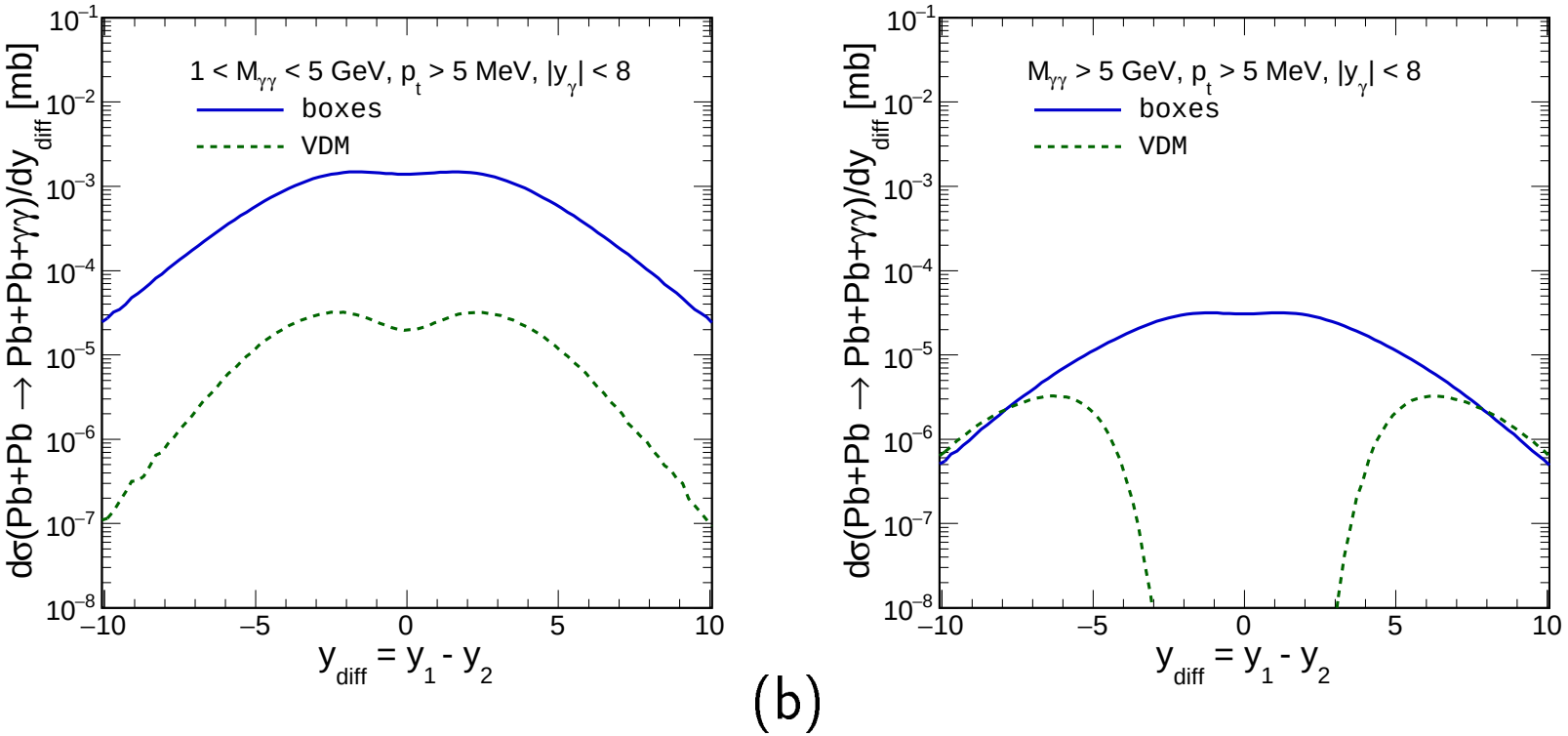

Figure: Distribution in y_{diff} for light-by-light scattering in PbPb$\to$PbPb$\gamma\gamma$. Here the transverse momentum cut is equal to 5 MeV. The blue solid line relates to the boxes, and the green dotted line to the VDM-Regge contribution. Here the range of measured di-photon invariant mass is: (a) $(1-5)$ GeV, (b) >5 GeV.

ALICE and FoCal

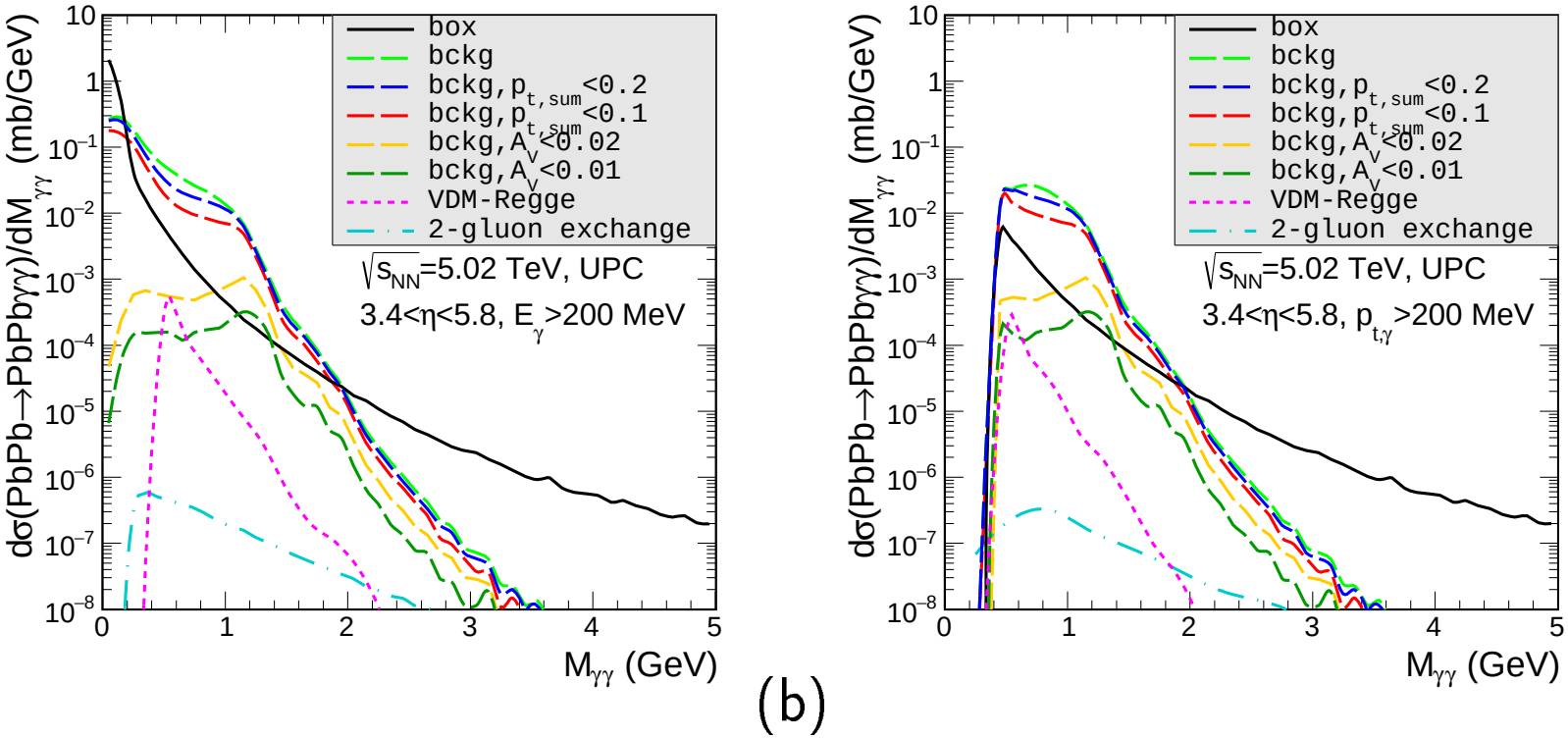

Figure: Invariant mass distribution for the nuclear process for the future FoCal:

(a) $E_{t,\gamma} > 200$ MeV and $3.4 < y_{\gamma_{1/2}} < 5.8$,

(b) $p_{t,\gamma} > 200$ MeV and $3.4 < y_{\gamma_{1/2}} < 5.8$.

Here, both photons are "measured" in FoCal. The background contribution is presented for different elimination cuts.

ALICE and FoCal

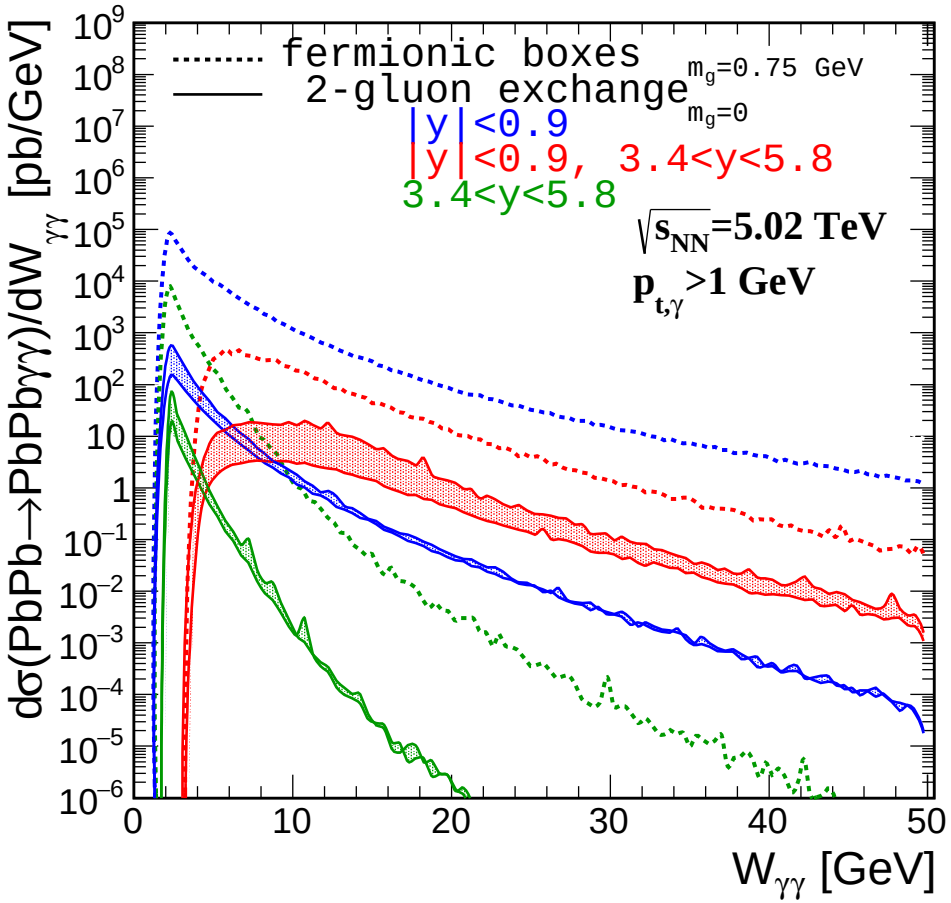

Figure: Di-photon invariant mass distribution for PbPb→PbPb$\gamma\gamma$ process for ALICE, FoCal and their combination.

ALICE and FoCal

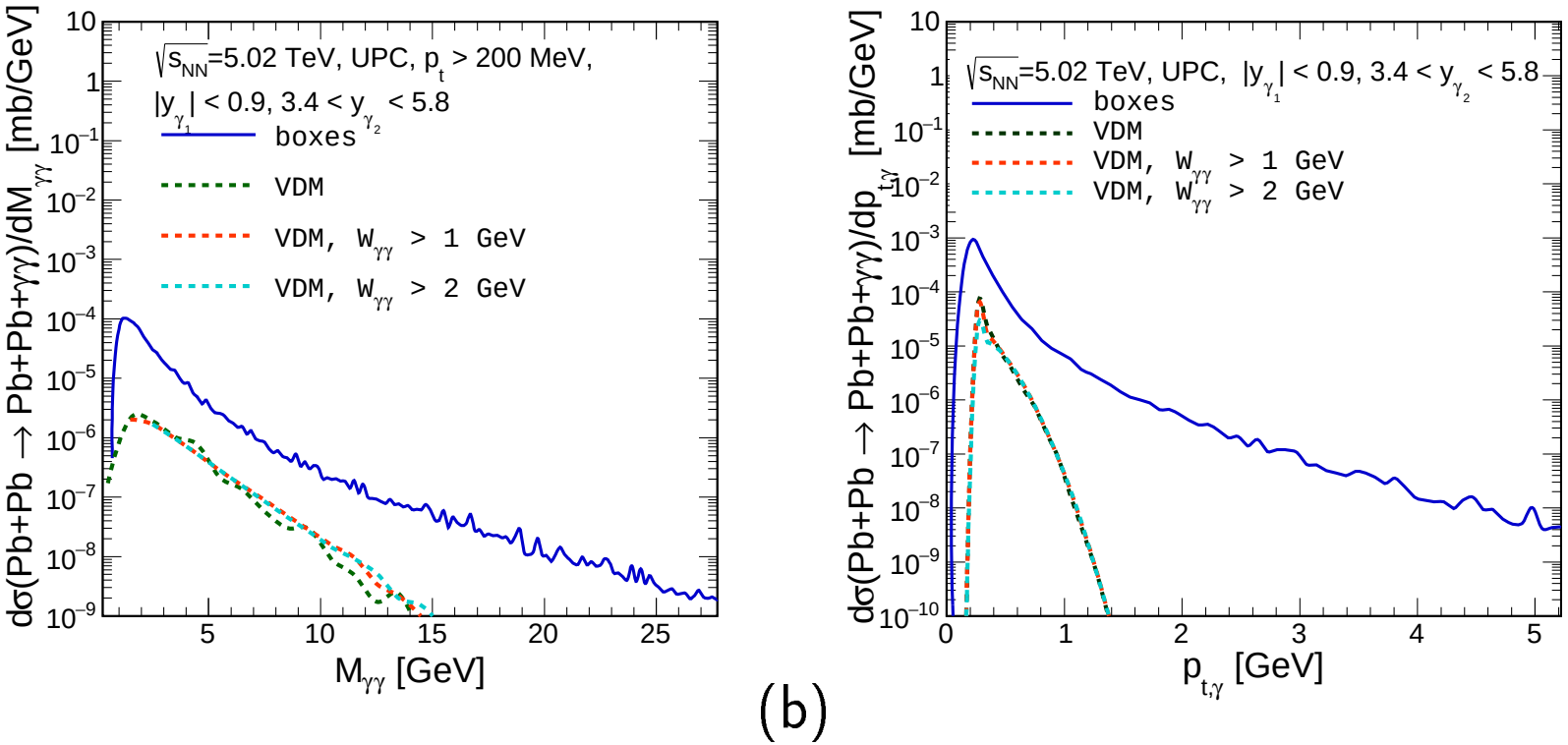

Figure: Prediction for the FoCal detector in association with mid-rapidity ALICE detector for photons: $p_t > 200$ MeV, di-photon mass $M_{\gamma\gamma} > 400$ MeV and photon rapidities $|y_1| < 0.9$ and $y_2 \in (3.4, 5.8)$. The blue line corresponds to fermionic loops and the green lines to the VDM-Regge contribution.

ALICE 3 kinematics

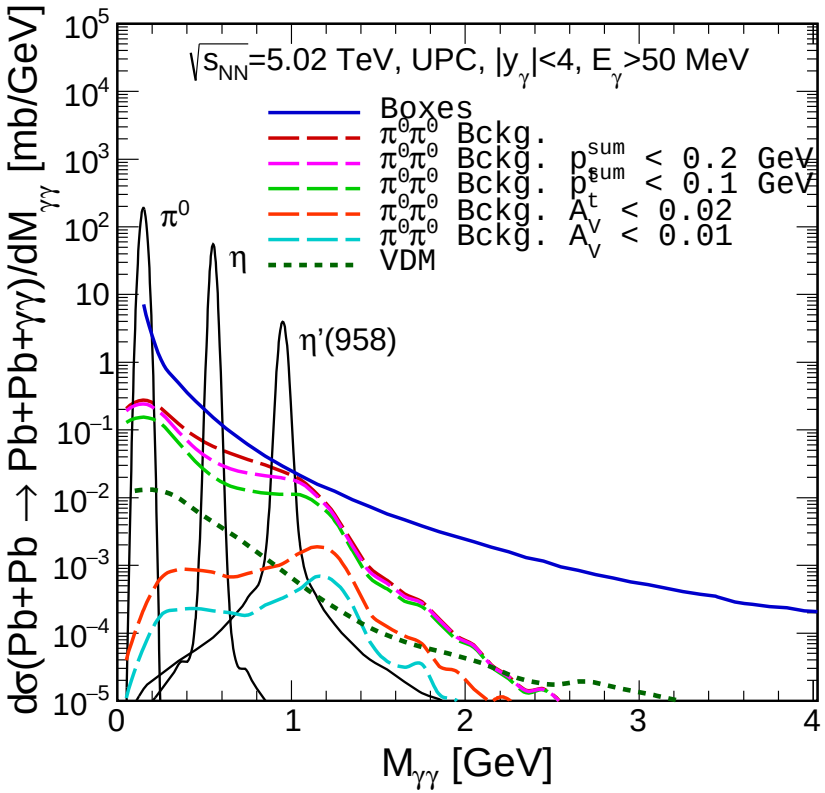

Figure: Di-photon invariant mass distribution for ALICE 3, i.e. rapidity $y_\gamma \in (-4, 4)$ and photon energy $E_\gamma > 50$ MeV.
Here the blue solid line relates to the box contribution, the dotted line to the VDM-Regge component and the dashed lines are for double-π^0 background

ALICE 3 kinematics

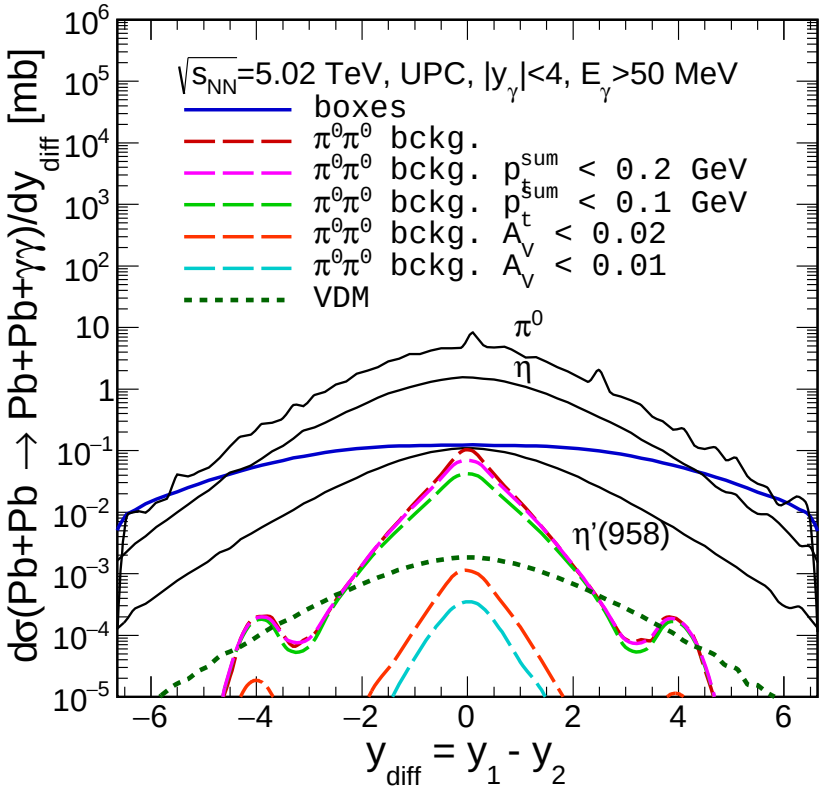

Figure: Differential cross section as a function of $y_{diff} = y_1 - y_2$ for extended ALICE 3 kinematics: $|y_\gamma| < 4$ and $E_\gamma > 50$ MeV.
Results are presented for boxes, resonances, VDM-Regge and double-π^0 background.

ALICE 3 kinematics

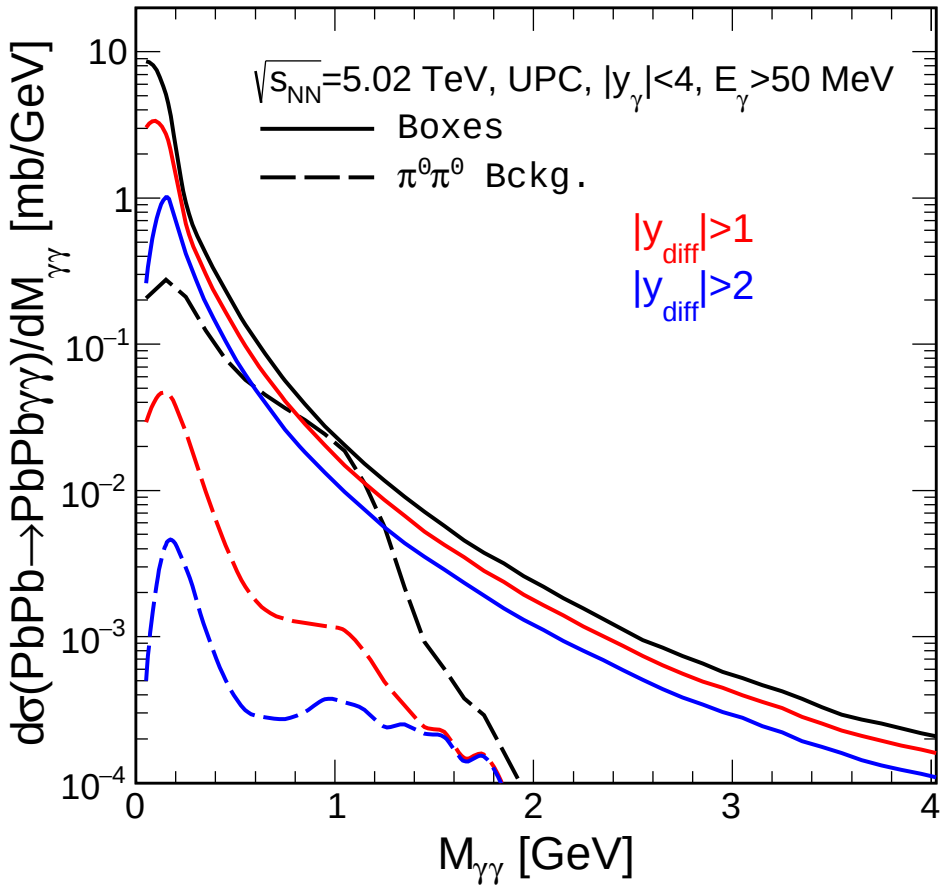

Figure: Influence of the $|y_{diff}|$ cut on the invariant $M_{\gamma\gamma}$ distribution.

ALICE 3 kinematics

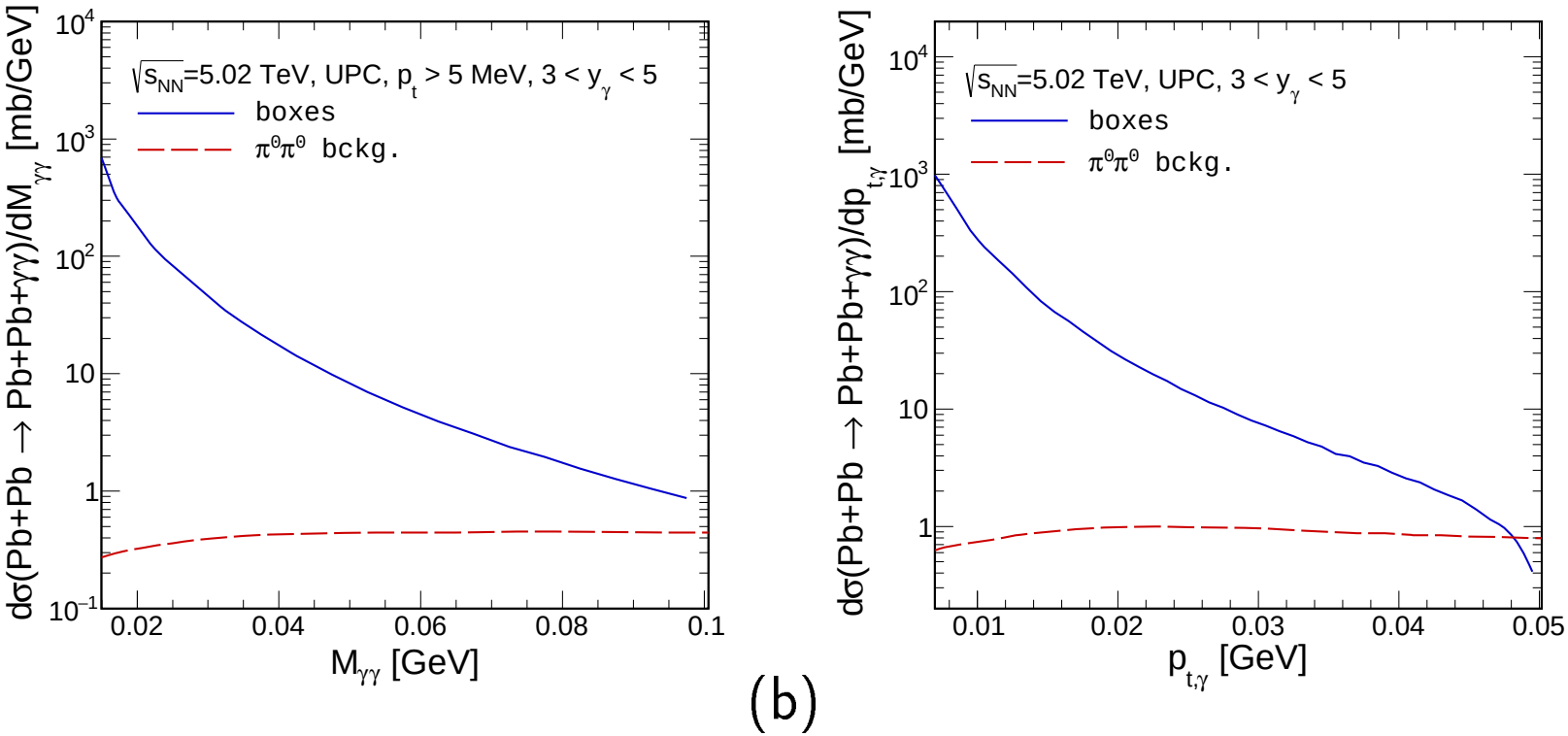

Figure: Prediction for the ALICE 3 experiment for soft photons: $p_t \in (5-50)$ MeV and photon rapidities $y_i \in (3,5)$. The blue line corresponds to fermionic loops, the red line relates to the double-π^0 background.

ALICE 3 kinematics

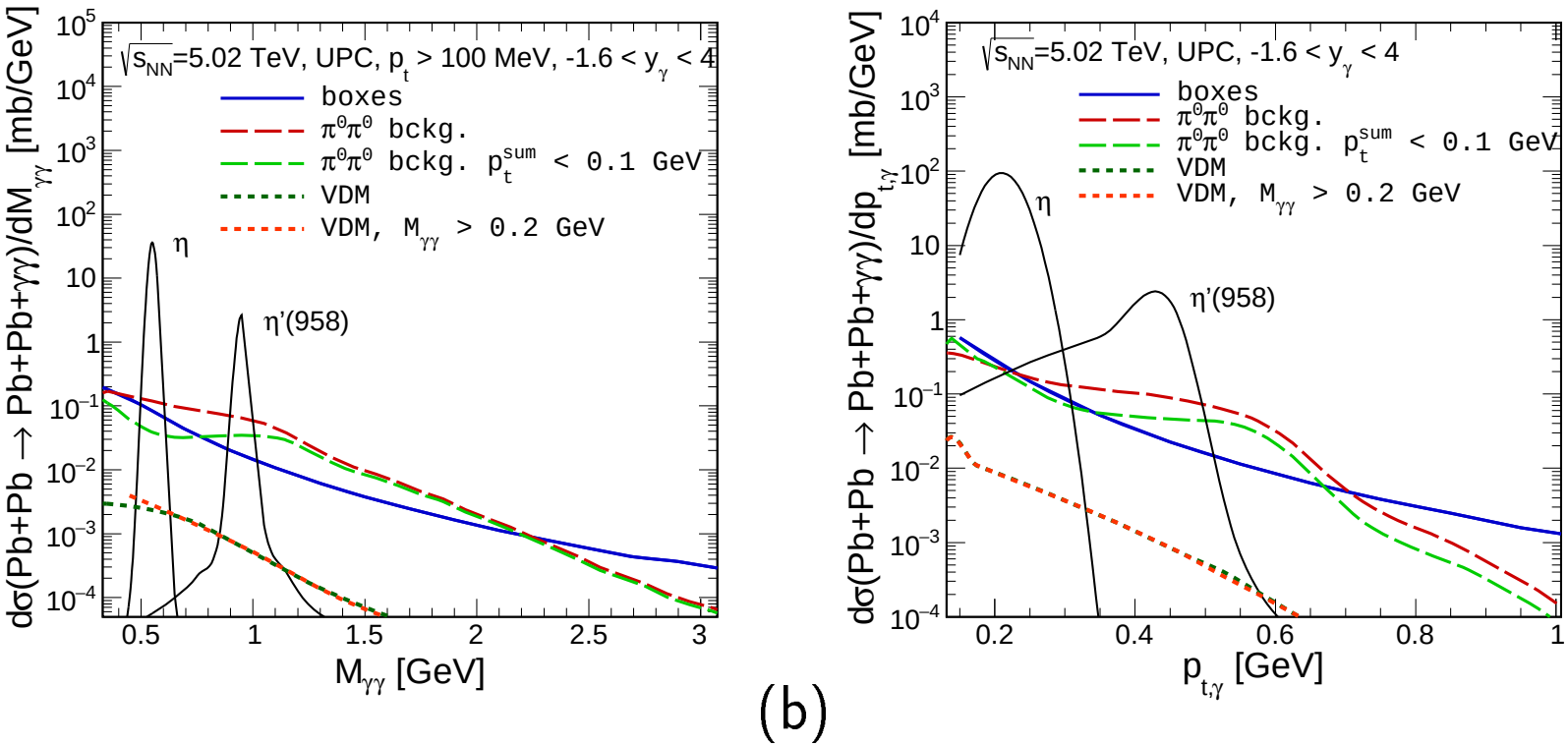

Figure: Prediction for the ALICE 3 experiment for photons: $p_t > 100$ MeV and photon rapidities $y_i \in (-1.6, 4)$. The blue line corresponds to fermionic loops, the red line relates to the double-π^0 background.

ALICE 3 kinematics

kinematical limitation			$\sigma(\pi^0\pi^0$ bckg) μb	σ(boxes) μb
p_t >5 MeV	$E_\gamma > 50$ MeV	$-4 < \eta_\gamma < 4$	112.824	952.590
$p_t > 100$ MeV	$E_\gamma > 50$ MeV	$-1.6 < \eta_\gamma < 4$	159.231	82.682
$p_t = (1 - 50)$ MeV	$E_\gamma > 50$ MeV	$3 < \eta_\gamma < 5$	105.301	3095.795

Table: Fermionic box signal contribution versus double-π^0 background given in μb at PbPb collision energy $\sqrt{s_{NN}} = 5.02$ TeV, with three considered scenarios of ALICE 3 detector limitations.

Conclusions

- We have investigated how to extend future studies of light-by-light scattering using future infrastructure (FoCal and ALICE 3).
- Several mechanisms of $\gamma\gamma \to \gamma\gamma$ scattering have been discussed.
- We have discussed shortly double photon fluctuation into vector mesons and Regge-type of interaction (VDM-Regge) as well as its interference with boxes. Negative interference was found.
- Combination of ALICE and FoCal can extend the range of $\gamma\gamma \to \gamma\gamma$ scattering to smaller energies.
- The special photon detector at $y \in (3,5)$ would allow to study the LbL scattering at very low energies and/or transverse momenta.
- The ways to eliminate unwanted double-π^0 background were discussed.
  (condition on $p_{t,sum}$, vector asymmetry, y_{diff})
- We have found that the background can be drastically reduced at large $|y_{diff}|$ which automatically means larger energies. This condition could be easily imposed using ALICE 3 detector.